Journal of Power Sources 192 (2009) 330–335

Contents lists available at ScienceDirect

Journal of Power Sources

journal homepage: www.elsevier.com/locate/jpowsour

Tungsten oxide nanowires grown on carbon paper as Pt electrocatalyst support for high performance proton exchange membrane fuel cells

Madhu Sudan Saha[a,1], Mohammad N. Banis[a], Yong Zhang[a], Ruying Li[a], Xueliang Sun[a,*], Mei Cai[b], Frederick T. Wagner[c]

[a] Department of Mechanical and Materials Engineering, The University of Western Ontario, 1151 Richmond Street N, London, Ontario, N6A 5B9, Canada
[b] General Motors Research and Development Center, Warren, MI 48090-9055, USA
[c] General Motors Research and Development, Honeoye Falls, NY 14472-1039, USA

ARTICLE INFO

Article history:
Received 30 January 2009
Received in revised form 2 March 2009
Accepted 3 March 2009
Available online 19 March 2009

Keywords:
Polymer electrolyte membrane fuel cells
Pt nanoparticles
$W_{18}O_{49}$ nanowires
Oxygen reduction reaction
Catalyst support

ABSTRACT

Tungsten oxide nanowires ($W_{18}O_{49}$ NWs) were directly grown on carbon paper by chemical vapor deposition. Well-dispersed Pt nanoparticles, with a size distribution from 2 to 4 nm, were deposited on the surface of $W_{18}O_{49}$ NWs through a simple reductive process. The resulting Pt/$W_{18}O_{49}$ NW/carbon paper composites formed a three-dimensional electrode structure. In comparison to conventional Pt/C electrocatalyst, the Pt/$W_{18}O_{49}$ NW/carbon paper composite exhibited higher electrocatalytic activity toward the oxygen reduction reaction and better CO tolerance in a single cell polymer electrolyte membrane fuel cell.

1. Introduction

In recent years, proton exchange membrane fuel cells (PEMFCs) have drawn a great deal of attention as alternative energy devices because of their high-energy conversion efficiency, low temperature, and zero emission of environmental pollutants [1,2]. Though tremendous progress has been made in the past decades, high cost and durability of the materials remain as big challenges for the commercialization of PEMFCs [2,3]. The cost can be reduced through several approaches such as reducing electrocatalyst loading and by achieving a more effective three-phase electrolyte–catalyst–gas phase boundary, thus leading to a better catalyst utilization at high current densities [4]. As Gasteiger et al. [2] pointed out, for automotive application, the current performance of state-of-the-art electrocatalyst (with H_2/air at 80 °C) is approximately 0.7 W cm^{-2} at 0.68 V (for 58% energy conversion), corresponding to 0.85 – 1.1 g_{Pt} kW^{-1} which requires to reduce to 0.2 g_{Pt} kW^{-1} at ≥0.65 V. In another report [5], cathode loadings of 0.05 mg cm^{-2} or less were one of the long-term goals set by U.S. Department of Energy for PEMFC performance in a 50 kW stack.

The catalytic activity of Pt-based catalysts depends on many factors, among which the catalyst-supporting material plays an important role. High surface area carbon black (e.g., Vulcan XC-72) is the most commonly used electrocatalyst support for Pt catalysts due to its high electrical conductivity and chemical stability. However, carbon black is also known to undergo electrochemical oxidation to surface oxides, and to CO_2 under fuel cell operating conditions [6]. As carbon corrodes, noble metal nanoparticles supported on carbon black will detach from the electrode and/or aggregate to larger particles, resulting in Pt surface area loss, which subsequently lowers the performance of PEMFCs [7]. In addition, Pt anode catalyst can be seriously poisoned by a small amount of carbon monoxide, thereby reducing the performance of the fuel cell [8,9]. Many groups have reported that the tolerance toward CO poisoning could be greatly improved by alloying Pt with an oxophilic element, such as ruthenium, tin, molybdenum and osmium [10–12]. This enhanced CO tolerance has been attributed to a modification of Pt electronic properties and surface chemistry to produce a bi-functional material. In the electronic effect, the addition of a second element provides modification of electronic interactions between the Pt and the CO adsorbate, resulting in a decreased Pt–CO bond strength and thus yielding more facile CO_{ads} electrooxidation [13]. In the bi-functional mechanism, the alloyed metal forms surface oxides at potentials much lower than that of Pt, providing local oxygen to oxidize the poisons to desorbing products [14].

* Corresponding author. Tel.: +1 519 661 2111x87759; fax: +1 519 661 3020.
E-mail addresses: mssaha@ymail.com (M.S. Saha), xsun@eng.uwo.ca (X. Sun).
[1] Present address: Queen's-RMC Fuel Cell Research Centre, 945 Princess Street, Kingston, Ontario, K7L 5L9, Canada.

0378-7753/$ – see front matter © 2009 Elsevier B.V. All rights reserved.
doi:10.1016/j.jpowsour.2009.03.011

Metal–metal oxide catalysts have been investigated as possible co-catalysts that are believed to operate via the bi-functional mechanism [9,15,16]. Specifically, tungsten oxides (WO_{3-x}) have been the subject of interest for this role and have been used as a support material for fuel cell catalysts [9,17–20]. It has been reported that catalysts made of Pt nanoparticles supported on WO_3 exhibit excellent CO tolerance [19,21] and higher catalytic activity. For example, the electrocatalytic activity of a Pt/WO_3 based electrode toward the oxygen reduction reaction in phosphoric acid was reported to be twice as high as that of Pt on carbon [22].

A great deal of attention has been given in recent years to develop nanomaterials with controlled nanostructures for improved fuel cell catalyst efficiency [23]. It is well known that the physical, electrochemical, electronic, and optical properties of nanostructured materials are different from those of bulk materials. One-dimensional nanostructures such as nanowires, nanobelts, nanotubes, and nanocables have attracted remarkable attention because of their unique electronic, magnetic, optical and mechanical properties and their wide range of potential applications in nanodevices [24]. Nanowires (NWs) consisting of metals, semiconductors, or inorganic compounds comprise one of the research directions that our group has been focusing on, such as the growth of SnO_2 NWs directly on carbon paper (fuel cell backing) as a catalyst support [25,26]. We have demonstrated that the Pt nanoparticles supported on SnO_2 NWs exhibited relatively higher electrocatalytic activity for oxygen reduction reaction than that of the Pt nanoparticles supported on carbon black [25].

So far, several methods have been reported to synthesize $W_{18}O_{49}$ NWs [27–29]. Shi et al. investigated the temperature dependence electrical transport properties of individual $W_{18}O_{49}$ NWs [29]. The conductivity of the $W_{18}O_{49}$ NWs is 2.58 Ω^{-1} cm^{-1} which is a little lower than that of bulk $W_{18}O_{49}$ (4 Ω^{-1} cm^{-1}) at room temperature [29,30]. The objectives of this paper are to directly grow $W_{18}O_{49}$ NWs on fuel cell backings as fuel cell catalyst supports to build three-dimensional (3D) electrode structures. The Pt nanoparticles were deposited on $W_{18}O_{49}$ NWs/carbon paper by reduction of Pt precursor with glacial acetic acid. The resultant composite electrodes of $Pt/W_{18}O_{49}$ NW/carbon paper were characterized by X-ray diffraction (XRD), scanning electron microscopy (SEM), transmission electron microscopy (TEM) and electrochemical techniques. Additionally, we will discuss the catalytic performance of Pt catalyst supported $W_{18}O_{49}$ NW/carbon paper composite toward oxygen reduction reaction and CO tolerance in PEMFCs.

2. Experimental

2.1. Growth of $W_{18}O_{49}$ nanowires

Before the growth of $W_{18}O_{49}$ NWs on carbon paper substrate, a thin tungsten film was first deposited on carbon microfibers of a carbon paper by RF magnetron sputtering using a tungsten target (purity 99.99%) in high purity argon (purity 99.999%). The chamber pressure was maintained at 4.6×10^{-3} Torr. After the sputtering, a thin 450 nm thick W film was obtained on carbon paper substrate. Subsequently, the sputtered carbon paper was placed in the middle part of a quartz tube, which was mounted horizontally inside a tubular furnace without using vacuum system. A carrier gas of high purity argon (99.999%) was passed through the quartz tube at a rate of 300 sccm (standard cubic centimeters per minute) through a hot water (90 °C) bath. After 20 min, the system was heated to 750 °C and was kept at this temperature for 30 min. Then the furnace was cooled down to room temperature in the flowing carrier gas. After the experiment, the colorless W film was observed to change to a dark purple-blue film; analysis of this film showed it to be an oxide, likely formed from reaction with adventitious air and/or water in the inert gas stream.

2.2. Deposition of Pt nanoparticles on $W_{18}O_{49}$ NW/carbon paper

Pt nanoparticles supported on $W_{18}O_{49}$ NW/carbon paper composites were prepared by the reduction of Pt precursors with glacial acetic acid as described previously [31]. In a typical preparation, the required amount of Pt precursor was added into 25 ml of glacial acetic acid, which was then agitated in an ultrasonic bath for 10 min. The $W_{18}O_{49}$ NWs/carbon paper was then soaked in the above solution, was heated to a temperature of 110 ± 2 °C, and was then kept at that temperature for about 5 h under constant stirring. Afterward, the Pt nanoparticles supported on $W_{18}O_{49}$ NWs/carbon paper ($Pt/W_{18}O_{49}$ NWs/carbon paper) composites were washed with deionized water and dried at 85 °C overnight in a vacuum oven. The Pt loadings of the $Pt/W_{18}O_{49}$ NW/carbon paper composites were determined by inductively coupled plasma-optical emission spectroscopy (ICP-OES). The morphologies of the composites were determined using a scanning electron microscope (SEM) (Hitachi S-2600 N) and transmission electron microscope (TEM) (Philips CM10). X-ray diffraction (XRD) analysis was also carried out with an X-ray diffractometer (Rigaku-MiniFlex) using Cu K_a radiation at 30 kV.

2.3. Electrochemical measurements

Cyclic voltammetry (CV) was conducted at room temperature using an Autolab potentiostat/galvanostat (Model, PGSTAT-30, Ecochemie, Brinkman Instruments) with a three-electrode, two-compartment configuration. A Pt wire and a reversible hydrogen electrode (RHE) were used as the counter and reference electrodes, respectively. For the measurement of hydrogen electrosorption curves, the potential was cycled between −0.0 and +1.2 V RHE at 50 mV s^{-1} to obtain the voltammograms of hydrogen adsorption in an Ar-purged 0.5 M H_2SO_4 aqueous solution. For CO stripping voltammetry, CO (99.5% in purity) was purged close to the working electrode for at least 30 min with the electrode polarized at 0.05 V vs. RHE in a fume hood. The electrode was then purged with pure N_2 for 30 min under potential control followed by voltammetric stripping.

2.4. Preparation and characterization of MEA

To fabricate a membrane electrode assembly (MEA), a $Pt/W_{18}O_{49}$ NWs NW/carbon paper composite with a Pt loading of 0.17 mg cm^{-2} was used as the cathode. A microporous layer was applied on the backside of the $W_{18}O_{49}$ NW/carbon paper composite according to the method reported by Kannan et al. [32]. Briefly, the ink for the microporous layer was prepared by ultrasonicating the required quantity of carbon black (Vulcan XC-72, Cabot) and polytetrafluoroethylene (PTFE) solution in a mixture of iso-propanol and deionized water (80:20 volume ratio) for 30 min followed by a magnetic stirring for about 1 h. The carbon loading was approximately 3.5 mg cm^{-2} and PTFE content was 30 wt.%. The microporous layer then was sintered at 350 °C in Ar for 1 h. It should be noted that this preparation procedure resulted in an unusual configuration: a catalyst layer on the side of the carbon paper against the membrane and a microporous layer on the side of the carbon paper next to the gas channels and current collector. For comparison, the commercial Pt/C electrocatalyst obtained from E-TEK (30 wt.% Pt on carbon black) was also used in the cathode for conventional electrode. Regarding the preparation of conventional electrode, carbon backing paper was first hydrophobically treated with polytetrafluoroethylene (PTFE) to reach a loading of 10 wt.% and then annealed at 350 °C in air. A microporous layer was then deposited onto the treated carbon paper with the same loadings of PTFE and carbon black in the $Pt/W_{18}O_{49}$ NW/carbon paper composite. A catalyst layer consisting of Pt/C catalyst, Nafion solution and iso-propanol

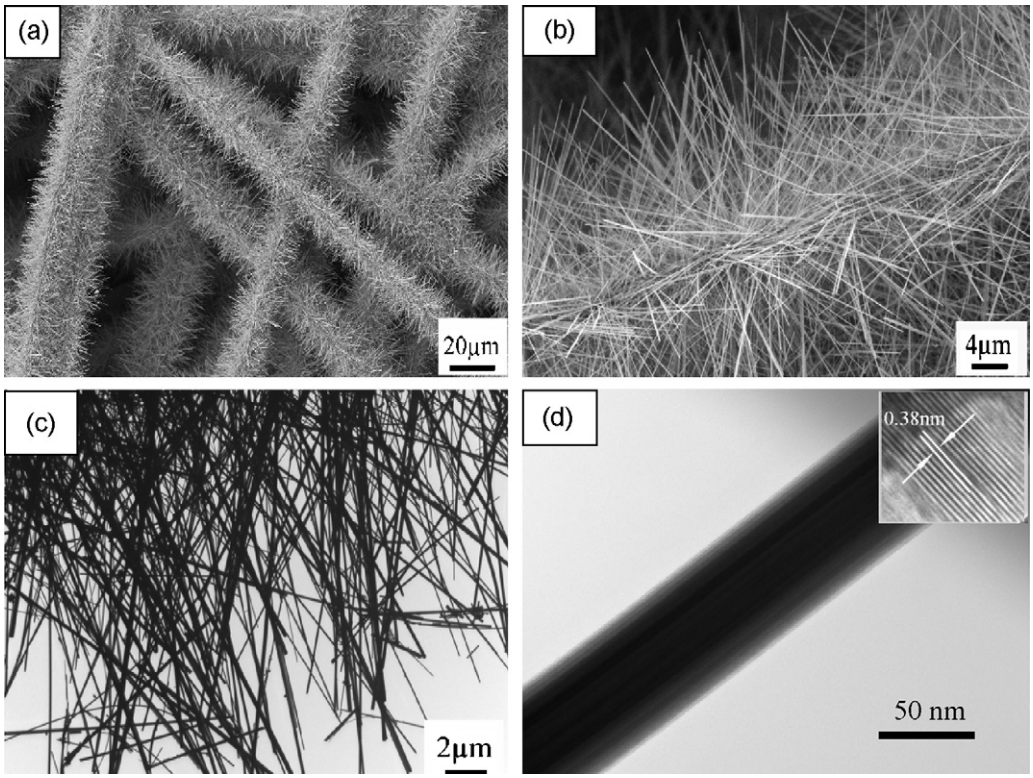

Fig. 1. SEM and TEM images of $W_{18}O_{49}$ NWs grown on carbon microfibers of carbon paper by chemical vapor deposition method. (a) Low magnification SEM image showing full coverage of $W_{18}O_{49}$ NWs on microfibers of carbon paper. (b) High magnification SEM image. (c) Low magnification TEM image of $W_{18}O_{49}$ nanowires. (d) TEM image showing individual $W_{18}O_{49}$ NWs. (Inset): High-resolution TEM image of a single NW.

was applied on the microporous layer. The ratio of dry Nafion to Pt/C was 1:3 by weight and the Pt loading was 0.20 mg cm^{-2}. The anodes were made with commercially available 30 wt.% Pt/C on single-sided ELAT with a Pt loading of 0.5 mg cm^{-2}. The electrode area was 1.0 cm^2, and typical loading of Nafion solution in all electrodes including the Pt/$W_{18}O_{49}$ NWs NW/carbon paper composite and the conventional electrodes was in the ranges of 0.6–0.8 mg cm^{-2} as a dry Nafion. Nafion 112 (DuPont Inc., USA) was used as the polymer electrolyte membrane. The MEA was fabricated in-house via hot pressing at 130 °C and 150 psig for 2 min. Polarization curves were obtained using a single fuel cell test station (Fuel Cell Technologies, Inc., USA).

3. Results and discussion

Fig. 1 shows the SEM and TEM images of $W_{18}O_{49}$ NWs grown on carbon microfibers of carbon paper. Low magnification SEM imaging reveals that high-density nanowires cover the carbon microfibers and form a three dimensionally hierarchical electrode structure, as shown in Fig. 1a. The obtained nanowires are very straight with average length of about 15 μm (Fig. 1b). TEM images show that the diameter of the nanowires is mostly in the range from 20 to 60 nm (Fig. 1c). Fig. 1d shows a typical bright field TEM image of a single nanowire with uniform diameter of 60 nm through the nanowire. The inset HRTEM image of the nanowire further reveals the single-crystalline nature of the nanowires and well-defined lattice fringe spacing of 0.38 nm perpendicular to the growth direction of the nanowire. This fringe corresponds to the (0 1 0) plane of the monoclinic $W_{18}O_{49}$ phase, indicating that the growth direction of the nanowire is along the [0 1 0] direction of $W_{18}O_{49}$. To identify phase structure of the obtained $W_{18}O_{49}$ NWs, XRD of the nanowires were performed as shown in Fig. 2. Besides the strong (0 0 2) graphite peak from carbon paper substrate, the sharp diffraction peaks labeled (*) in Fig. 2 were identified as the pure monoclinic $W_{18}O_{49}$ (JCPDS05-0392), and the peaks labeled (♦) were assigned to residual metallic tungsten. Therefore, XRD analyses indicate that the resultant nanowires are composed of single-crystalline $W_{18}O_{49}$ NWs.

Fig. 3a–c shows typical TEM images of $W_{18}O_{49}$ NWs/carbon paper after deposition of Pt nanoparticles at different loadings using different concentrations of Pt precursor. The concentrations of Pt precursor used for this study are 1, 2 and 4 mM, resulting in corresponding Pt loadings of 0.08, 0.17 and 0.31 mg cm^{-2} on NWs. It was clearly observed that Pt nanoparticles were well dispersed on the surface of the $W_{18}O_{49}$ NWs/carbon paper. The density of Pt particles increases with the increase of the concentrations of Pt precursors and the size of Pt particles are from 2 to 4 nm.

The electrochemical adsorption/desorption properties of Pt nanoparticles on Pt/$W_{18}O_{49}$ NW/carbon paper composites were examined by CV as shown in Fig. 4a. For comparison, the commercially available 30 wt.% Pt/C electrocatalyst was also examined

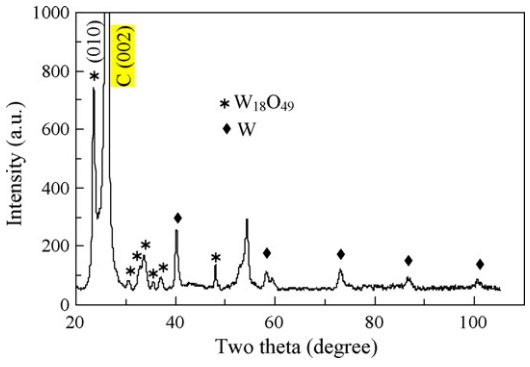

Fig. 2. XRD pattern of $W_{18}O_{49}$ NWs grown directly on carbon paper.

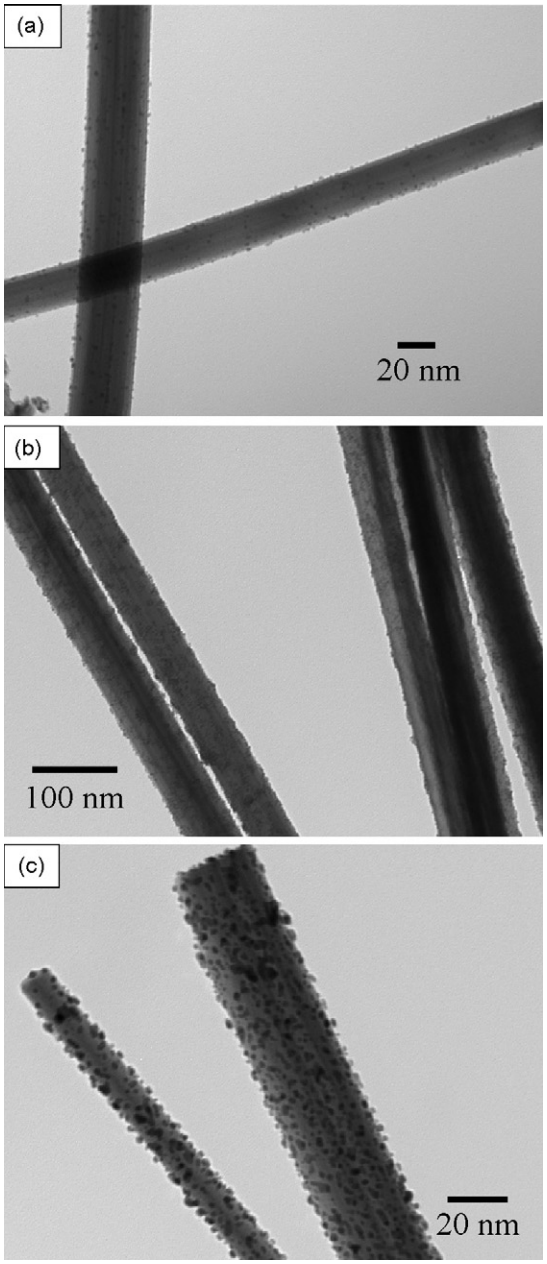

Fig. 3. TEM images of Pt nanoparticles deposited on the $W_{18}O_{49}$ NWs/carbon paper from different concentrations of Pt precursor (a) 1 mM, (b) 2 mM and (c) 4 mM in glacial acetic acid. The corresponding Pt loadings on the NWs are 0.08, 0.17 and 0.31 mg cm^{-2}.

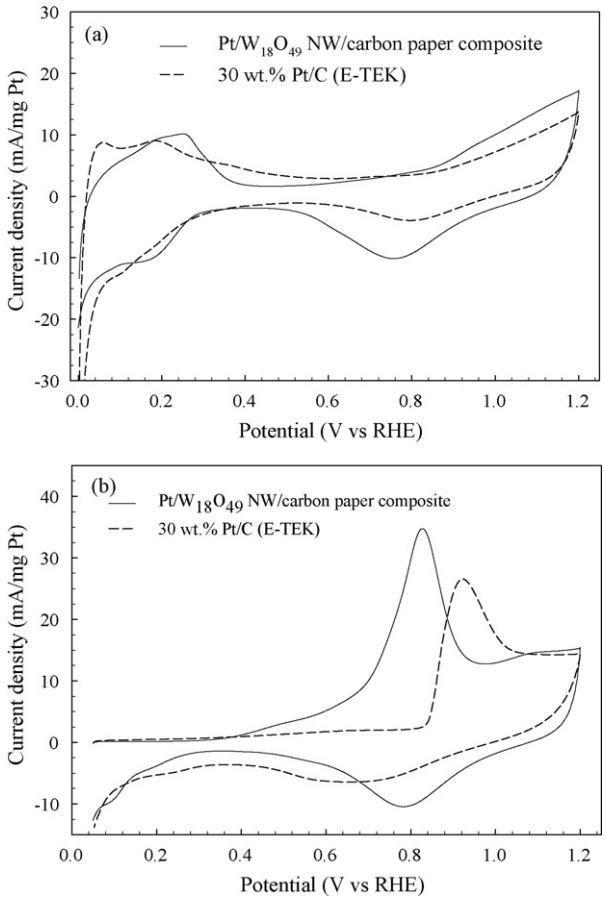

Fig. 4. CVs of $Pt/W_{18}O_{49}$ NW/carbon paper composite electrode (a) in the absence and (b) presence of CO in 0.5 M H_2SO_4 aqueous solution at room temperature. Potential scan rate: 50 mV s^{-1}. The CO was absorbed at 0.05 V for 30 min, subsequently, the solution CO was removed by Ar bubbling for 30 min while maintaining the potential at 0.05 V vs. RHE. A representative CV of a standard 30 wt.% Pt/C electrode is included for reference. Current densities normalized with respect to the Pt loading.

under the same conditions. The currents were normalized on the basis of Pt loading. The voltammetric features of both electrodes reveal the typical characteristics of Pt metal [33], with Pt oxide formation in the +0.8 to +1.2 V range, the reduction of Pt oxide at *ca.* +0.78 V, and the adsorption and desorption of hydrogen between 0.35 and 0 V. The electrochemical active areas of both $Pt/W_{18}O_{49}$ NW/carbon paper composite and commercial Pt/C electrodes were determined from the CVs (Fig. 4a). By integrating the charge in the hydrogen adsorption/desorption region, we found that the active surface area is larger for the $Pt/W_{18}O_{49}$ NW/carbon paper composite than the Pt/C electrode. This difference is attributed to the unique 3D structure of the $Pt/W_{18}O_{49}$ NW/carbon paper composite, as we reported previously [34], and well dispersed Pt nanoparticles with sizes of 2–4 nm on the surface of $W_{18}O_{49}$ NWs.

Fig. 4b shows adsorbed CO (CO_{ads}) stripping voltammograms for the $Pt/W_{18}O_{49}$ NWs/carbon paper composite along with one of a commercial Pt/C electrode in 0.5 M H_2SO_4 solution at 50 mV s^{-1}. CO was purged while holding the potential at 0.05 V vs. RHE for 30 min at 25 °C. The observed CO-stripping peak potential of 0.81 V for the $Pt/W_{18}O_{49}$ NW/carbon paper composite is slightly more negative than the 0.93 V seen for the Pt/C electrode under the same conditions. This result suggests that the CO_{ads} oxidation is energetically more favorable at the $Pt/W_{18}O_{49}$ NW/carbon paper composite electrode than at the Pt/C electrode. In the case of the $Pt/W_{18}O_{49}$ NW/carbon paper composite, the shift of the CO-stripping peak potential in negative direction (Fig. 4b) may indicate that the CO tolerance is related to the electrochemical desorption of CO promoted by active tungsten hydrous oxides, in agreement to the bi-functional mechanism proposed previously [35,36].

Fig. 5a shows Tafel plots comparing the oxygen reduction activity of the 0.17 mg_{Pt} cm^{-2} $Pt/W_{18}O_{49}$ NW/carbon paper composite on the cathode of an MEA to that of a 0.2 mg_{Pt} cm^{-2} reference Pt/C catalyst. The ohmic resistance in the electrode and electrolyte was evaluated by a non-linear least-square fit of the semi-empirical equation proposed by Ticianelli et al. [37]. Both MEAs used commercial 0.5 mg_{Pt} cm^{-2} E-TEK electrodes as anodes. The data were taken at 80 °C, with anode/cathode flows of 200 and 100 sccm H_2 and O_2, respectively, at 100%/100% relative humidity and 25/30 psig backpressures. At the 900 mV (*iR*-corrected) recommended as a standard reporting condition in Ref. [2], the $Pt/W_{18}O_{49}$ catalyst

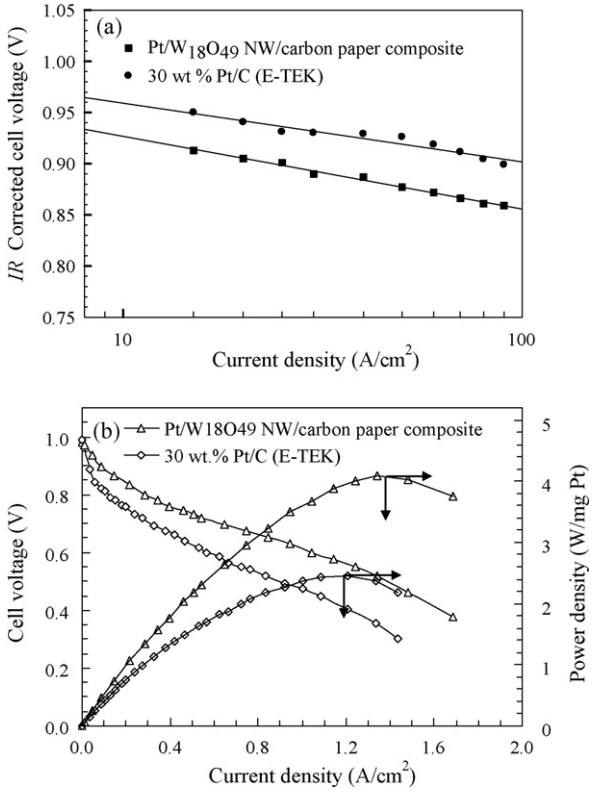

Fig. 5. (a) Comparison of the *iR*-free Tafel plots for oxygen reduction reaction. (b) Polarization curves and power density curves in single cell PEMFC of MEA's made with $Pt/W_{18}O_{49}$ NW/carbon paper composite (0.17 mg_{Pt} cm^{-2}) and conventional Pt/C electrode (0.20 mg_{Pt} cm^{-2}) as cathodes for H_2/O_2 at 80 °C, Nafion 112 membrane, 25/30 psig anode and cathode back pressure, respectively. Anodes were E-TEK gas diffusion electrode with a Pt loading of 0.5 mg_{Pt} cm^{-2}.

gave ~4-fold higher current than the Pt/C reference for nearly the same Pt loading. In terms of activity per mass of Pt at 900 mV, the $Pt/W_{18}O_{49}$ catalyst gave 0.63 A mg_{Pt}^{-2} vs. the 0.13 A mg_{Pt}^{-2} for the Pt/C reference in this work. The enhancement in the activity for oxygen reduction on $Pt/W_{18}O_{49}$ NWs/carbon paper composite is attributed to the uniform dispersion of smaller Pt particles, an improved catalyst-support binding and a synergistic effect of $W_{18}O_{49}$ NWs as catalyst support. This reference catalyst result is numerically similar to the 0.11–0.16 A mg_{Pt}^{-2} shown in Ref. [2] to be representative of state-of-the-art Pt/C catalysts, but the data in Ref. [2] were taken at much lower pressure (150 kPa absolute) than used in this work. Given the 46 kPa_{abs} partial pressure of water vapor at 80 °C, the 25/30 psig backpressures used here correspond to 228 and 262 kPa_{abs} partial pressures for hydrogen and oxygen, respectively. These compare to the 104/104 kPa_{abs} partial pressures used in Ref. [2]. Neyerlin et al. [38] have shown that, at a constant cell potential, the current density due to oxygen reduction for a Pt/C catalyst varies with the 0.79 power of pO_2 and the 0.5 power of pH_2. Therefore, to correct the 0.13 A mg_{Pt}^{-2} measured here at high pressure for the reference Pt catalyst down to the established reference conditions of Ref. [2], one divides by $(228/104)^{0.5} \times (262/104)^{0.79} = 3.07$. The Pt/C reference activity measured here, corrected to the standard conditions of Ref. [2], is therefore 0.042 A mg_{Pt}^{-2}, about 1/3 of the established state-of-the-art activity for Pt/C, perhaps due to low utilization of Pt and/or contamination in this home-made electrode. The $Pt/W_{18}O_{49}$ catalyst mass activity measured here, corrected to the standard conditions of Ref. [2], is 0.20 A mg_{Pt}^{-2}, a bit higher than state-of-the-art Pt/C activity. These data therefore do suggest an enhancement of Pt kinetic mass activity by the $W_{18}O_{49}$ nanowire support. The magnitude of the enhancement implied by these data depends on the extent to which the factors that suppressed the Pt/C activity here below the state-of-the-art level also suppressed the activity of the $Pt/W_{18}O_{49}$.

The H_2/O_2 performance of the membrane electrode assembly (MEA) using the 0.17 mg_{Pt} cm^{-2} $Pt/W_{18}O_{49}$ NW/carbon paper as the cathode and a 0.5 mg_{Pt} cm^{-2} E-TEK electrode as the anode was evaluated in a 1 cm^2 single-cell PEMFC, as shown in Fig. 5. For comparison, the polarization curve of the conventional MEA made with 0.20 mg_{Pt} cm^{-2} of the commercial 30 wt.% Pt/C catalyst as the cathode and another 0.5 mg_{Pt} cm^{-2} E-TEK electrode as the anode is also presented. Polarization characteristics were compared at 80 °C with 25/30 psig backpressure for the anode and cathode, respectively, and humidification to 100% relative humidity. As can be seen in Fig. 4a, the MEA made with $Pt/W_{18}O_{49}$ NW/carbon paper composite showed much better performance than this conventional Pt/C MEA. At a fixed cell voltage of 0.6 V, the current density of $Pt/W_{18}O_{49}$ NW/carbon paper composite electrode is 1.04 A cm^{-2}, which is higher by a factor of 1.8 relative to the Pt/C electrode (0.56 A cm^{-2}). However, it should be noted that the performance of the Pt/C electrode falls well below that of state-of-the-art PEMFCs operating under similar, high-pressure H_2/O_2 conditions. All practical terrestrial applications of fuel cells will use air rather than pure oxygen as the oxidant. The nitrogen in air strongly exacerbates the transport limitations that can become substantial at high current densities, and it is difficult to accurately emulate transport conditions in a full-scale fuel cell in a cell with only 1 cm^2 active area, as used here. Therefore, fully reliable evaluation of these promising $Pt/W_{18}O_{49}$ NWs catalysts at high current densities will require synthesis of enough material to run multiple 50 cm^2 cells under representative H_2/air conditions and comparison to true state-of-the-art Pt/C electrodes, as is planned.

4. Conclusions

In summary, the composite electrodes of Pt nanoparticles supported on $W_{18}O_{49}$ NW/carbon paper were prepared by growing $W_{18}O_{49}$ NWs on carbon paper followed by reduction of Pt precursors with glacial acetic acid. TEM images show that the Pt nanoparticles were uniformly dispersed on the surface of NWs, with a particle size of 2–4 nm. The $Pt/W_{18}O_{49}$ NW/carbon paper composite electrode shows higher kinetic activity for oxygen reduction reaction in a 1 cm^2 single cell and higher CO tolerance than that of conventional Pt/C electrode. Such nanowire-based 3D electrodes can be extended to other material classes and therefore may open a new door to fabricate novel electrodes with improved performance, lower cost and higher CO tolerance for PEMFCs and direct methanol fuel cells.

Acknowledgements

This research was supported by General Motors of Canada, Natural Sciences and Engineering Research Council of Canada, Canada Research Chair Program, Canada Foundation for Innovation, Ontario Early Researcher Award and the University of Western Ontario.

References

[1] R. Borup, J. Meyers, B. Pivovar, Y.S. Kim, R. Mukundan, N. Garland, D. Myers, M. Wilson, F. Garzon, D. Wood, P. Zelenay, K. More, K. Stroh, T. Zawodzinski, X.J. Boncella, J.E. McGrath, O.M. Inaba, K. Miyatake, M. Hori, K. Ota, Z. Ogumi, S. Miyata, A. Nishikata, Z. Siroma, Y. Uchimoto, K. Yasuda, K.-I. Kimijima, N. Iwashita, Chem. Rev. 107 (2007) 1–48.
[2] H.A. Gasteiger, S.S. Kocha, B. Sompalli, F.T. Wagner, Appl. Catal. B: Environ. 56 (2005) 9–35.
[3] P. Costamagna, S. Srinivasan, J. Power Sources 102 (2001) 253–269.
[4] S. Srinivasan, E.A. Ticianelli, C.R. Derouin, A. Redondo, J. Power Sources 22 (1988) 359–375.
[5] A.T. Haug, R.E. White, J.W. Weidner, W. Huang, S. Shi, T. Stoner, N. Rana, J. Electrochem. Soc. 149 (2002) A280–A287.

[6] K.H. Kangasniemi, D.A. Condit, T.D. Jarvic, J. Electrochem. Soc. 151 (2004) E125–E132.
[7] J.G. Liu, Z.H. Zhou, X.X. Zhao, Q. Xin, G.Q. Sun, B.L. Yi, Phys. Chem. Chem. Phys. 6 (2004) 134.
[8] R.A. Lemons, J. Power Sources 29 (1990) 251–264.
[9] E.J. McLeod, V.I. Birss, Electrochim. Acta 51 (2005) 684–693.
[10] K. Wang, H.A. Gasteiger, N.M. Markovic, P.N. Ross, Electrochim. Acta 41 (1996) 2587–2593.
[11] J. Divisek, H.F. Oetjen, V. Peinecke, V.M. Schmidt, U. Stimming, Electrochim. Acta 43 (1998) 3811–3815.
[12] M. Watanabe, S. Motoo, Electrochemistry 44 (1976) 602–607.
[13] B. Hammer, J.K. Norskov, Surf. Sci. 343 (1995) 211–220.
[14] M. Watanabe, S. Motoo, Electroanal. Chem. Interf. Electrochem. 60 (1975) 267–272.
[15] K. Lasch, L. Jorrisen, J. Garche, J. Power Sources 84 (1999) 225–230.
[16] J. Long, R. Stroud, K. Swider-Lyons, D. Rolison, J. Phys. Chem. B 104 (2000) 9772–9776.
[17] P.K. Shen, A.C.C. Tseung, J. Electrochem. Soc. 141 (1994) 3082–3090.
[18] M. Gotz, H. Wendt, Electrochim. Acta 43 (1998) 3637–3644.
[19] S. Jayaraman, T.F. Jaramillo, S.-H. Baeck, E.W. McFarland, J. Phys. Chem. B 109 (2005) 22958–22966.
[20] H. Chhina, S. Campbell, O. Keslerc, J. Electrochem. Soc. 154 (2007) B533–B539.
[21] F. Maillard, E. Peyrelade, Y. Soldo-Olivier, M. Chatenet, E. Chainet, R. Faure, Electrochim. Acta 52 (2006) 1958–1967.
[22] O. Savadogo, P. Beck, J. Electrochem. Soc. 143 (1996) 3842–3846.
[23] R. Narayanan, M.A. El-Sayed, Nano Lett. 4 (2004) 1343–1348.
[24] Z.L. Wang, Nanowires and Nanobelts: Materials, Properties and Devices, Kluwer–Academic, Boston, MA, 2003.
[25] M.S. Saha, R. Li, M. Cai, X. Sun, Electrochem. Solid-State Lett. 10 (2007) B130–B133.
[26] M.S. Saha, R. Li, X. Sun, Electrochem. Commun. 9 (2007) 2229–2234.
[27] Y. Li, Y. Bando, D. Goldberg, Adv. Mater. 15 (2003) 1294–1296.
[28] S.J. Wang, C.H. Chen, R.M. Ko, Y.C. Kuo, C.H. Wong, C.H. Wu, K.M. Uang, T.M. Chen, B.W. Liou, Appl. Phys. Lett. 86 (2005) 2631031–2631033.
[29] S. Shi, X. Xue, P. Feng, Y. Liu, H. Zhao, T. Wang, J. Crystal Growth 310 (2008) 462–466.
[30] E. Salje, B. Güttler, Philos. Mag. B 50 (1984) 607–620.
[31] M.S. Saha, R. Li, X. Sun, J. Power Sources 177 (2008) 314–322.
[32] A.M. Kannan, V.P. Veedu, L. Munukutla, M.N. Ghasemi-Nejhad, Electrochem. Solid-State Lett. 10 (2007) B47–B50.
[33] A.J. Bard, L.R. Faulkner, Electrochemical Methods, Fundamentals and Applications, Wiley, New York, 1980.
[34] X. Sun, R. Li, D. Villers, J.P. Dodelet, S. Desilets, Chem. Phys. Lett. 379 (2003) 99–104.
[35] K. Machida, M. Enyo, G. Adachi, J. Shiokawa, J. Electrochem. Soc. 135 (1988) 1955–1961.
[36] A.K. Shukla, M.K. Ravikumar, A.S. Arico, G. Candiano, V. Antonucci, N. Giordano, A. Hamnett, J. Appl. Electrochem. 25 (1995) 528–532.
[37] E.A. Ticianelli, C.R. Derouin, A. Redondo, S. Srinivasan, J. Electrochem. Soc. 135 (1988) 2209–2214.
[38] K.C. Neyerlin, W. Gu, J. Jorne, H.A. Gasteiger, J. Electrochem. Soc. 153 (2006) A1955–A1963.